Geophysical Journal International

Geophys. J. Int. (2011) **185,** 85–92 doi: 10.1111/j.1365-246X.2011.04946.x

Crustal V_p–V_s ratios and thickness for Ross Island and the Transantarctic Mountain front, Antarctica

Marco Finotello,[1] Andrew Nyblade,[1] Jordi Julia,[1] Douglas Wiens[2] and Sridhar Anandakrishnan[1]

[1]*Department of Geosciences, Penn State University, University Park,* PA 16802, *USA. E-mail: nyblade@psu.edu*
[2]*Department of Earth and Planetary Sciences, Washington University, St. Louis,* MO 63130, *USA*

Accepted 2011 January 4. Received 2011 January 4; in original form 2010 February 23

SUMMARY

We investigate crustal V_p–V_s ratios and thickness along the Transantarctic Mountain (TAM) front and on Ross Island, Antarctica to determine if the TAM crust has been modified by the Neogene magmatism associated with Ross Island. A seismic low velocity zone (LVZ) in the upper mantle beneath Ross Island extends laterally ∼80 km under the TAM front, and mantle temperatures within the LVZ may be sufficiently elevated for partial melting to have occurred and modified the crust. Data for the study come from 16 temporary seismic stations that were part of the TAM Seismic Experiment and three permanent stations. Estimates of V_p/V_s (κ) and crustal thickness (H) have been obtained from receiver functions analysed using the H–κ stacking method for 10 of the stations, and for the remaining stations, crustal thickness has been calculated by using the Moho P_s arrival time with an assumed V_p/V_s value. A V_p/V_s value of 1.88 is obtained for Ross Island, consistent with the mafic composition of the volcanic rocks from Mt. Erebus. V_p/V_s values for stations in the TAM situated away from the LVZ range from 1.63 to 1.78, with a mean of 1.73, while values for stations in the TAM lying above the LVZ range from 1.67 to 1.78, with a mean of 1.72. This result indicates that there is little difference in bulk crustal composition for areas above and away from the LVZ, and together with a V_p/V_s value (1.73) that is typical for felsic to intermediate composition crust, suggests that the crust along the TAM front has not been altered significantly by mafic magmatism. Crustal thickness estimates along the coast are quite variable, ranging from 18 to 33 km, and increase to 39 km inland beneath the crest of the TAM. On Ross Island, crustal thickness estimates range between 19 and 27 km.

Key words: Crustal structure; Antarctica.

1 INTRODUCTION

In this study, we investigate crustal structure along the Transantarctic Mountain (TAM) front in the vicinity of Ross Island, Antarctica, to determine the extent to which the crust has been modified by the Neogene volcanism associated with Ross Island and the Terror Rift. The TAM represent Earth's largest non-collisional mountain range and mark the tectonic boundary between the East Antarctic (EA) craton and the West Antarctic Rift System (WARS; Fig. 1). Extension within the WARS began during the Jurassic and continues today within the Terror Rift (Behrendt *et al*. 1991a,b; Fig. 1). Mafic to intermediate alkaline volcanism is present at Mt. Erebus, located on Ross Island at the southern end of the Terror Rift.

P- and *S*-wave tomography models (Watson *et al*. 2006), as well as surface wave tomography models (Lawrence *et al*. 2006a), reveal a low velocity zone (LVZ) in the upper mantle beneath and surrounding Ross Island. Laterally, the LVZ extends from north of Ross Island to ∼80 km inland from the coast beneath the TAM (Fig. 1). The LVZ, which extends from the uppermost mantle to least 150 km depth, indicates that upper-mantle temperatures over a broad area may be elevated by ∼200–300 K, sufficiently high to cause partial melting (Watson *et al*. 2006). Consequently, the crust and upper mantle surrounding Ross Island may have been altered over a much broader region than suggested by the spatial extent of the volcanism (Fig. 1). To determine if the crust away from Ross Island has been modified by the Neogene magmatism, we obtain new estimates of V_p/V_s and crustal thickness from receiver function (RF) analysis using broad-band data from 16 stations on Ross Island and along the TAM front that were part of the Transantarctic Mountain Seismic Experiment (TAMSEIS), as well as from three permanent stations.

2 GEOLOGICAL SETTING AND BACKGROUND

The initial uplift of the TAM began at ∼55 Ma (Fitzgerald 1992, 1994). The TAM basement consists of Precambrian and Cambrian metasediments, Cambro-Ordovician granites and Devonian

© 2011 The Authors
Geophysical Journal International © 2011 RAS

GJI Geodynamics and tectonics
Downloaded from https://academic.oup.com/gji/article/185/1/85/606263 by guest on 09 April 2024

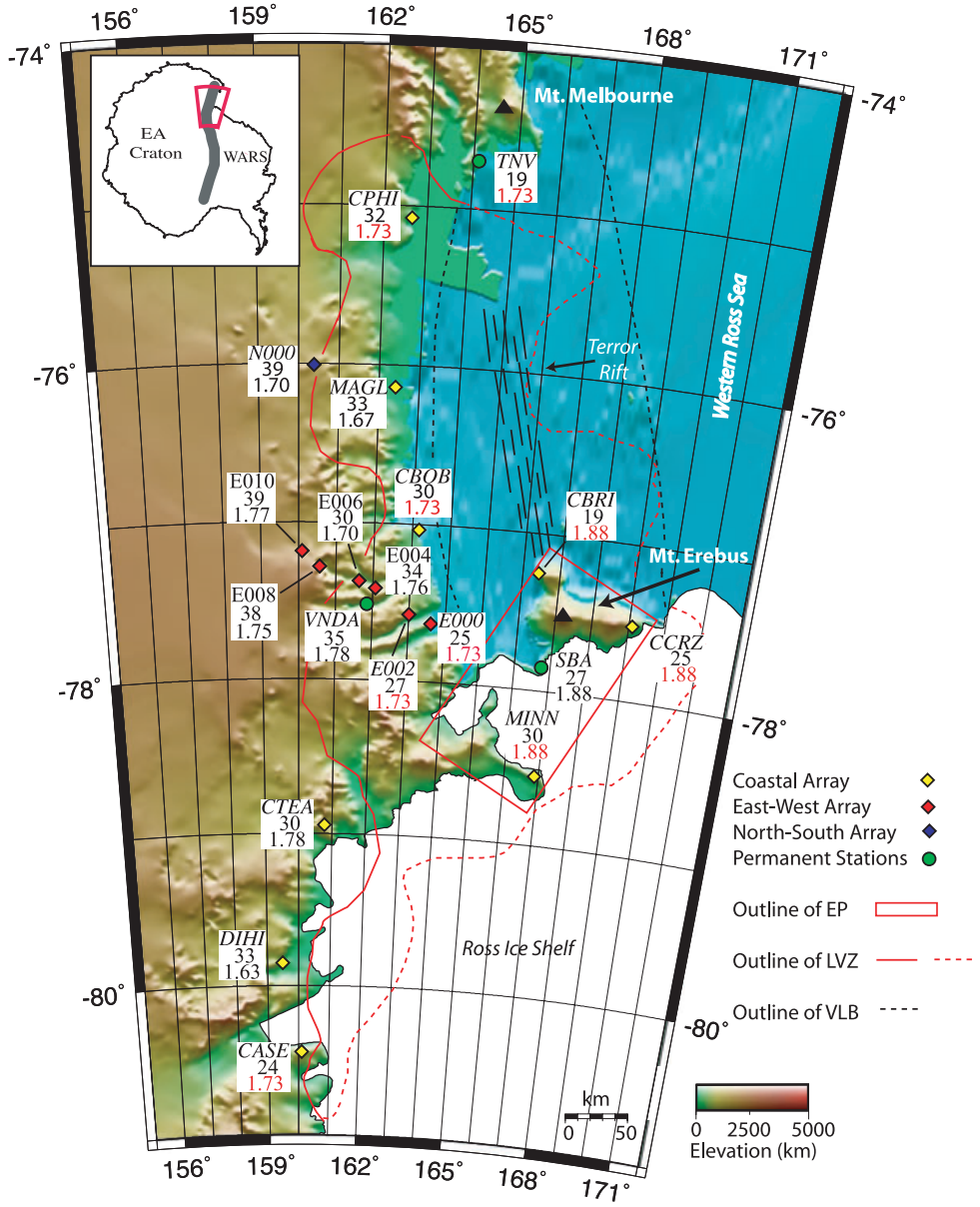

Figure 1. Topographic map of the TAM showing seismic station locations and results from this study. The red box outlines the general extent of the Erebus volcanic province and the thin red line marks the extent of a –1 per cent *S*-wave velocity anomaly (LVZ) from Watson *et al*. (2006). The eastern edge of the LVZ is marked with a dashed line because it is not well defined. EA, East Antarctica; WARS, West Antarctic Rift System. Crustal thickness estimates (km) and V_p–V_s ratios are given below each station name. A V_p–V_s ratio in red indicates that it was assumed. Inset shows a map of Antarctica with the study area highlighted. The TAM are marked by the grey line.

granodiorites (Fitzgerald 1992). The basement complex was eroded to form the Kurki peneplain before being overlain by the Devonian-Triassic Beacon Supergroup, which consists of shallow marine, glacial and alluvial sediments (Barrett *et al*. 1986). Magmatism within the TAM occurred at ∼180 Ma with the intrusion of the Ferrar dolerite sills and the eruption of the Kirkpatrick basalt (Fitzgerald 1992).

Ross Island sits at the southern end of the Victoria Land Basin (VLB) in the western Ross Sea (Fig. 1). High crustal *P*-wave velocities and gravity modelling results indicate that the VLB crust has been extensively intruded and thinned (Trey *et al*. 1999). Presently, extension is thought to be occurring in the Terror rift, which formed by transtensional and strike-slip faulting in the early Neogene (Behrendt *et al*. 1991b, 1996). The Terror Rift lies 50–100 km east of the TAM front in the VLB, is ∼70 km wide, and stretches from Mt. Erebus to Mt. Melbourne (Cooper *et al*. 1987; Paulsen and Wilson 2009; Fig. 1). Mt. Erebus is located in the middle of Ross Island, at one end of the Terror Rift (Fig. 1). It marks the northernmost extent of the Erebus Volcanic Province (EVP), which extends south of Ross Island to Minna Bluff (station MINN; Kyle 1990a,b; Cooper *et al*. 2007; Fig. 1). The composition of lava flows forming Mt. Erebus ranges from basanite to anorthoclase phonolite (Kyle *et al*. 1992).

Several studies have investigated crustal thickness beneath the TAM using RFs (Bannister *et al*. 2003; Lawrence *et al*. 2006b; Pondrelli *et al*. 1997). Bannister *et al*. (2003) used data from a 10-station temporary array plus data from permanent stations VNDA and SBA to compute RFs using the multiple-taper spectral

Downloaded from https://academic.oup.com/gji/article/185/1/85/606263 by guest on 09 April 2024

correlation method of Park and Levin (2000). Lawrence *et al*. (2006b) investigated crustal structure using data from the TAMSEIS network along with data from three permanent stations SBA, TNV and VNDA. They used a niching genetic algorithm to jointly invert RFs and Rayleigh wave phase velocities for crustal and upper-mantle structure. Both studies report crustal thicknesses of ∼20 km for Ross Island and along the TAM front adjacent to Ross Island, and thicker crust (36–40 km) beneath the TAM.

Pondrelli *et al*. (1997) used data from a four station temporary array that crossed perpendicular to the strike of the TAM approximately along 76°S, near TAMSEIS stations MAGL and N000 (Fig. 1). They obtained Moho depth estimates of 26 km near the coast and 41–43 km beneath the crest of the TAM. Della Vedova *et al*. (1997) used data from 58 portable stations to conduct a wide angle seismic refraction experiment along the ACRUP transect which also ran along 76°S. Using forward ray trace modelling and traveltime inversion, Della Vedova *et al*. (1997) obtained Moho depth estimates of ∼38 km beneath the crest of the TAM which decreased to ∼30 km at the coast.

3 DATA, METHODS AND RESULTS

Data for this study comes from 16 TAMSEIS stations and three permanent stations located on Ross Island and along the TAM front above the upper-mantle LVZ imaged by Watson *et al*. (2006) and Lawrence *et al*. (2006a,b) (Fig. 1). The TAMSEIS network consisted of 41 three-component, broad-band seismometers that were deployed from 2000 November until 2003 December. The stations were configured in three arrays: Coastal, East–West and North–South (Fig. 1). Data from nine stations of the Coastal array, including two stations on Ross Island, six in the East–West array and one station from the North–South array have been used, along with data from the permanent stations SBA, TNV and VNDA. All of these stations were located on bedrock, while the remaining TAMSEIS stations were located on ice. Additional information about the TAMSEIS network can be found in Lawrence *et al*. (2006a).

RF analysis is commonly used to obtain constraints on crust and upper-mantle structure beneath three-component seismic stations (e.g. Langston 1979). In this study, the iterative time-domain deconvolution method of Ligorría and Ammon (1999) was used to generate the RFs from a range of backazimuths (see Supporting Information). The RFs were then filtered with a Gaussian pulse width of 1.0 ($f \leq 0.5$ Hz) or 2.5 ($f \leq 1.25$ Hz), and the radial and transverse components were inspected for evidence of lateral heterogeneity. Events with large amplitude transverse RFs were removed from the data set (Finotello 2009). A least-squares misfit criterion was also applied to evaluate the quality of the RFs, and those with a fit of 85 per cent and higher were used for modelling and interpretation. A cut-off of 85 per cent resulted in only a few RFs for stations TNV, CCRZ, CBOB, CBRI and so for these stations, RFs with a minimum fit of 75 per cent were used.

The H–κ stacking method was then applied to the RFs to estimate crustal thickness (H) and the V_p/V_s (κ; Zhu and Kanamori 2000). In this method, to find the optimal H and κ, RFs are stacked such that they are transformed from the time domain into objective function values in H–κ parameter space. The objective function used in the Zhu and Kanamori (2000) method involves the summation over the RFs of the weighted amplitudes of each phase at the predicted arrival times for different values of H and κ

$$s(H,\kappa) = \sum_{i=1}^{N} [w_1 A_i(t_1) + w_2 A_i(t_2) - w_3 A_i(t_3)], \quad (1)$$

where w_1, w_2, w_3 are weights ($\Sigma w_i = 1$) assigned to the amplitude, A_i, of each respective phase and t_1, t_2 and t_3, are the predicted arrival times of the Moho P_s, P_pP_s and $P_sP_s + P_pS_s$ phases. N is the number of RFs. When $s(H, \kappa)$ reaches a maximum, the optimal values for H and κ have been found that fit the simple one-layer crustal model (Zhu and Kanamori 2000).

To apply the H–κ method, weights must be assigned to each phase in eq. 1, and an average crustal V_p must be selected. A V_p of 6.5 km s^{-1}, which is consistent with average crustal P-wave velocities from previous studies (Della Vedova *et al*. 1997; Pondrelli *et al*. 1997), and a weighting system of $w_1 = 0.5$, $w_2 = 0.5$ and $w_3 = 0.0$ were used. The third weight (w_3) was set to be zero because it was difficult to consistently identify a clear second crustal reverberation ($P_sP_s + P_pS_s$) on the RFs at every station (Figs 2–4 and Supporting Information).

Results for two stations are shown in Figs 2 and 3. For most stations, as illustrated for station CTEA, RFs computed using a Gaussian pulse width of 1.0 were used (Fig. 2). For station SBA, however, RFs with a Gaussian pulse width of 1.0 did not yield consistent arrivals for the Moho P_s and crustal reverberations. Therefore, RFs computed with a Gaussian pulse width of 2.5 was used instead to avoid interference with arrivals from other possible intracrustal discontinuities (Fig. 3). Results for the other stations can be found in the Supporting Information.

Uncertainties in H and κ were obtained simultaneously using a bootstrap method, which involved repeating the stacking procedure 200 times with a resampled data set selected at random from the original data set (Efron and Tibshirani 1991). Examples of the uncertainties are shown in Figs 2 and 3. In addition, for assessing uncertainty in crustal thickness and V_p/V_s resulting from the choice of the mean crustal P-wave velocity, the H–κ stacks were recomputed using mean crustal P-wave velocities of 6.3 km s^{-1} and 6.7 km s^{-1}. To obtain an overall uncertainty in H and κ, the uncertainty obtained from the bootstrap method was combined with the range of H and κ values obtained when using different mean crustal P-wave velocities, respectively. Results and the overall uncertainties for the 10 stations where the H–κ stacking method was successfully applied are summarized in Table 1 and Fig. 1.

For nine stations, the H–κ stacking method did not yield acceptable results mainly because the crustal multiples (P_pP_s and $P_sP_s + P_pS_s$) could not be clearly identified on RFs generated with either a Gaussian pulse width of 1.0 or 2.5 (Fig. 4 and Supporting Information). Therefore, for those stations, the method described by Zandt *et al*. (1995) was followed to estimate H using the arrival time of the Moho P_s phase and an assumed V_p/V_s value. An assumed V_p/V_s value of 1.73, which is an average of V_p/V_s values from the stations in Table 1 excluding SBA, was used for all stations located outside the EVP. For the stations located within the EVP (CBRI, CCRZ and MINN; Fig. 1), a V_p/V_s value of 1.88 was used to be consistent with the H–κ stacking result from SBA. The results are summarized in Table 2 and Fig. 1, and the uncertainty associated with crustal thickness estimates in Table 2 represent two standard deviations of the mean value.

4 DISCUSSION

In this section, we first examine crustal V_p/V_s to investigate the influence of Neogene magmatism on crustal composition, and then comment on crustal thickness. We note that the V_p/V_s values obtained are not likely affected by dipping structure along the TAM front because most of the events come from backazimuths that are

Downloaded from https://academic.oup.com/gji/article/185/1/85/606263 by guest on 09 April 2024

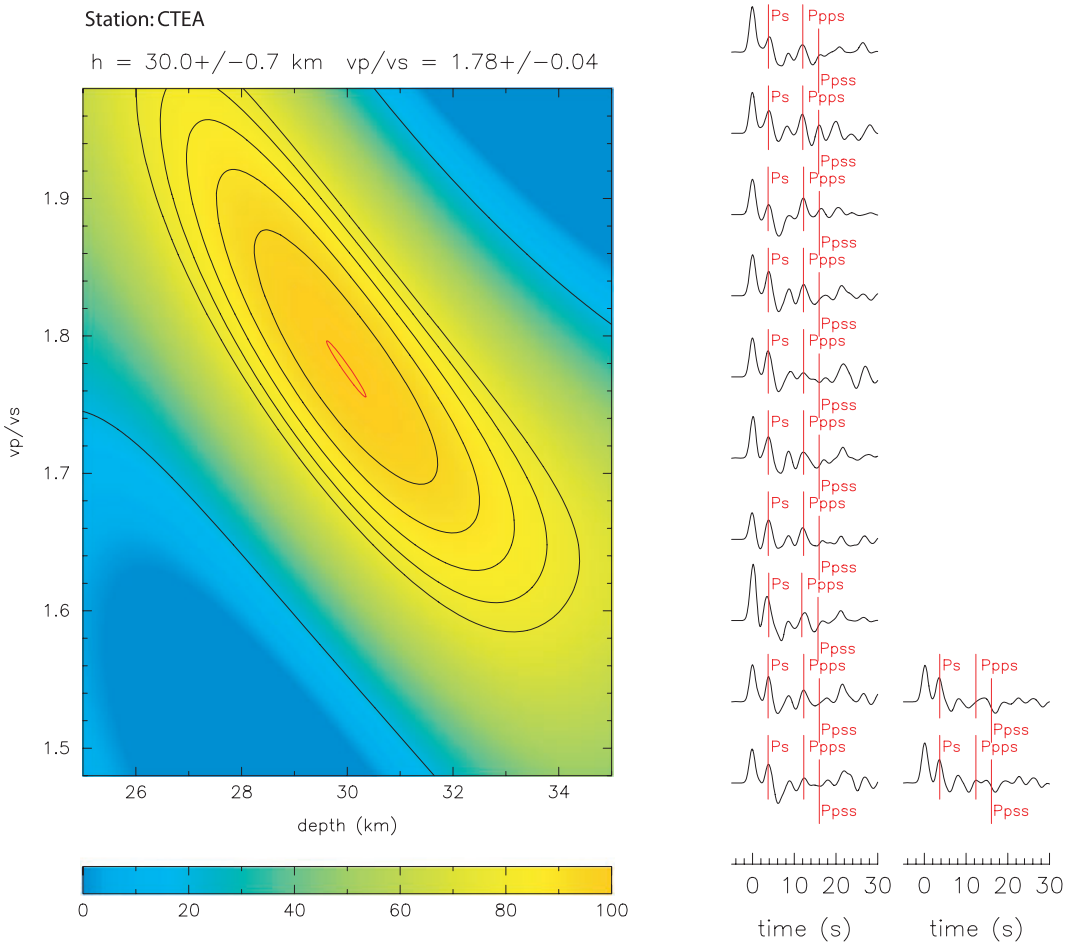

Figure 2. Result of H–κ stacking of receiver functions for station CTEA. Left-hand side: stacking surface where contours show percentage values of the objective function and the red line gives 90 per cent confidence ellipse. Right-hand side: receiver functions with labelled arrivals of relevant phases predicted by best fitting H and κ shown with red lines. Receiver functions have been computed using a Gaussian pulse width of 1.0.

generally along strike of the front (Supporting Information). V_p/V_s is commonly used as a general indicator of bulk crustal composition. Typical V_p/V_s values for different lithologies are on average ∼1.70 for felsic rocks (i.e. granite), ∼1.76 for intermediate rocks (i.e. diorite) and ∼1.84 for mafic rocks (i.e. basalt), and are little influenced by subsolidus temperature variations (Christensen 1996).

The V_p/V_s value of 1.88 obtained for station SBA on Ross Island indicates a bulk crustal composition that is mafic, which is consistent with the composition of volcanic rocks on the island. V_p/V_s values for stations in the TAM situated away from the LVZ (i.e. E010, E008, CTEA, DIHI; Fig. 1) range from 1.63 to 1.78, with a mean of 1.73, while values for stations in the TAM lying above the LVZ (i.e. E006, VNDA, E004, MAGL, N000; Fig. 1) range from 1.67 to 1.78, with a mean of 1.72. This comparison shows that there is little difference in bulk crustal composition for areas above and away from the LVZ, and together with a mean V_p/V_s (1.72) which is typical for felsic to intermediate composition crust, suggests that the crust along the TAM front has not been altered significantly by mafic magmatism. If a significant portion of the crust had been modified by mafic intrusions and/or underplating, then V_p/V_s values closer to the V_p/V_s ratio of 1.88 found at Station SBA would be expected across regions of the TAM front lying above the LVZ.

Is it possible that there could be minor modification of the crust under parts of the TAM front that is small enough to go undetected? If significant compositional modification (e.g. over 5–10 km) of the lowermost crust had occurred, then a gradational transition across the crust–mantle interface would be expected. A clear Moho P_s can be seen on the RFs for all of the stations, and, in addition, the multiples from the Moho can also be seen clearly on many of the stations, even for those stations situated above the LVZ (Supporting Information). If the crust–mantle interface were gradational over a depth interval of more than ∼5 km, then a clear Moho P_s arrival, as well as multiples from the Moho, would not be readily observed. Thus, while a few kilometres of lower crustal modification cannot be ruled out, larger amounts of crustal modification by mafic intrusions and/or underplating are not consistent with the nature of the arrivals on the RFs or with V_p/V_s values obtained.

A comparison of the V_p/V_s values for the TAM crust to values for Precambrian crust of similar age on other Gondwanan continents corroborates further the conclusion that the TAM crust above the LVZ has not been significantly modified. For example, Pan African crust in East Africa that has not been affected by Cenozoic rifting has an average V_p/V_s ratio of 1.75 (Dugda *et al*. 2005).

Along the East–West array, crustal thickness estimates range from ∼25 km near the coast to ∼39 km beneath the crest of the TAM (Fig. 1). Along the Coastal array and TAM front, crustal thickness is quite variable ranging between 18 and 33 km. In comparison to results from previous studies, near the crest of the TAM our results (stations E004–E010 and VNDA) are consistent with the Moho depths reported by Bannister *et al*. (2003) and Lawrence

Downloaded from https://academic.oup.com/gji/article/185/1/85/606263 by guest on 09 April 2024

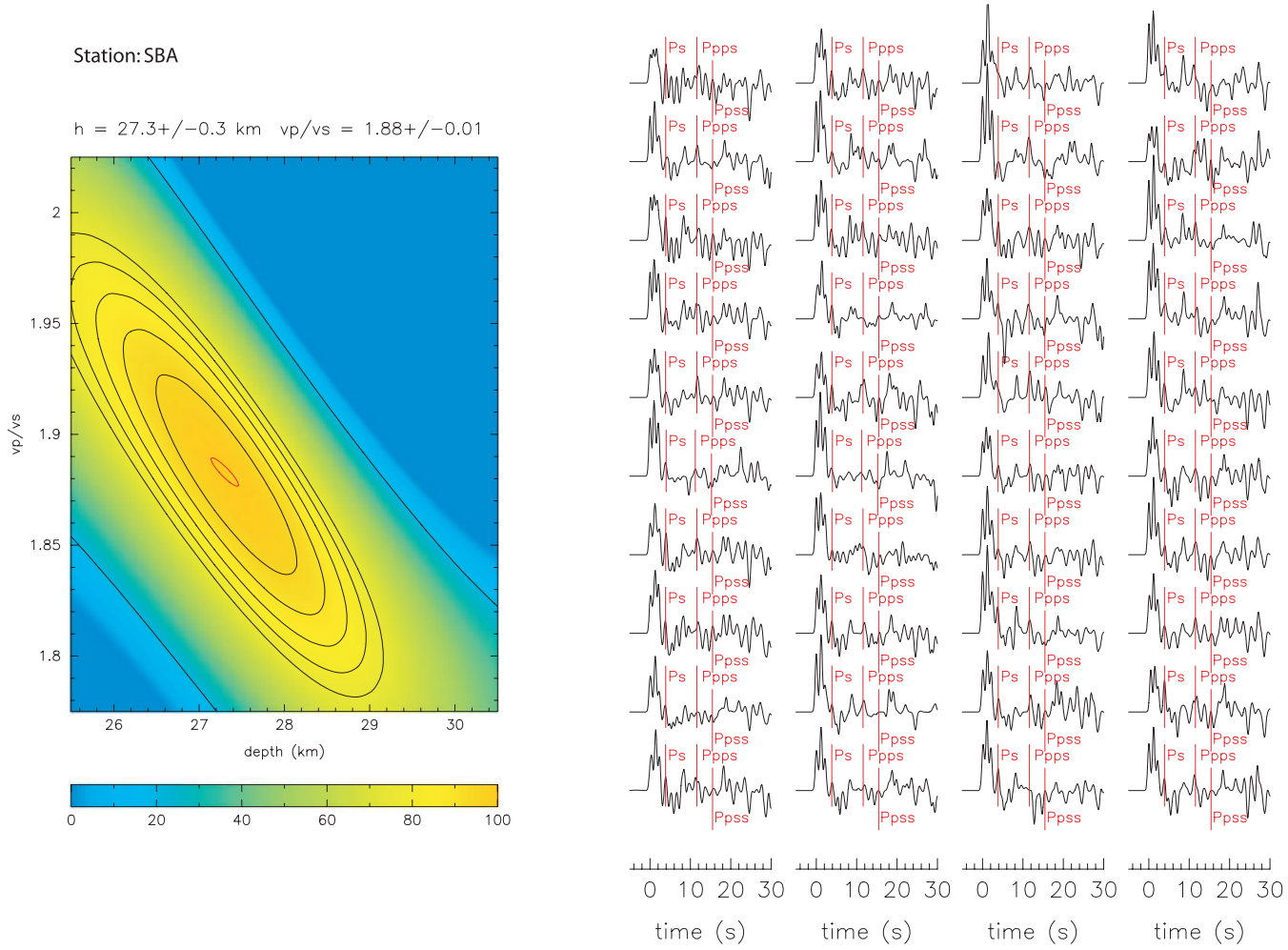

Figure 3. Result of H–κ stacking of receiver functions for station SBA. Left-hand side: stacking surface where contours show percentage values of the objective function and the red line gives the 90 per cent confidence ellipse. Right-hand side: Selected receiver functions with labelled arrivals of relevant phases predicted by best fitting H and κ shown with red lines. Receiver functions have been computed using a Gaussian pulse width of 2.5.

et al. (2006b) (Table 1 and Fig. 1). However, near station E000 along the coast, Bannister *et al*. (2003) reported a crustal thickness of ∼18 km, but we find a ∼25 km thick crust beneath station E000. In the velocity model obtained by Bannister *et al*. (2003) from inverting RFs, a Moho depth of ∼18 km corresponds to an *S*-wave velocity increase to 4.0–4.2 km s^{-1}. Their model also shows that at ∼25 km depth there is an *S*-wave velocity increase to 4.3–4.4 km s^{-1}, which is consistent with our Moho depth estimate for station E000.

Bannister *et al*. (2003) suggested that the transition between the VLB and TAM near Ross Island is characterized by a rapid change in crustal thickness from ∼20 km to ∼40 km. Although the majority of the ray coverage in our data set is parallel to this transition, our results indicate that this transition may not be quite as pronounced, with only a change in crustal thickness from ∼25 to ∼40 km. Bannister *et al*. (2003) also commented on crustal V_p/V_s but noted that it was not well constrained in their models. At station VNDA they reported a V_p/V_s value of ∼1.76, which is consistent with our result.

Lawrence *et al*. (2006b) also used the TAMSEIS data set to estimate crustal thickness beneath the TAM. Along the East–West Array, our results are consistent with the crustal thickness estimates reported by Lawrence *et al*. (2006b) except beneath two stations. At stations E000 and E004 our results indicate a crustal thickness of ∼25 km and ∼35 km, respectively, both ∼5 km thicker than reported by Lawrence *et al*. (2006b). Similarly, for the Coastal array stations, excluding TNV and CASE, our crustal thickness estimates are, on average, between 8 and 10 km thicker than those reported by Lawrence *et al*. (2006b). At stations CASE and TNV, our results are consistent with Lawrence *et al*. (2006b), within the large uncertainties in our Moho depth estimates for these stations (Table 2).

There are two possible explanations for the difference between our crustal thickness estimates and those of Lawrence *et al*. (2006b). The first one has to do with how Lawrence *et al*. (2006b) interpreted their velocity models. For example, at station E000, Lawrence *et al*. (2006b) placed the Moho at ∼20 km depth, and on their velocity model, this depth coincides with an *S*-wave velocity increase from ∼3.45 to 4.1 km s^{-1}. Our results indicate a deeper Moho (25 km, Table 2), which coincides with an *S*-wave velocity increase in the Lawrence *et al*. (2006b) model for this station from 4.1 to 4.45 km s^{-1}. There are similar discrepancies in the interpretation of the velocity models for stations CBOB, CTEA and MAGL.

The second explanation concerns station DIHI, where the difference in crustal thickness could be due to the low average crustal V_s (∼3.1 km s^{-1}) in the Lawrence *et al*. (2006b) model compared to

Downloaded from https://academic.oup.com/gji/article/185/1/85/606263 by guest on 09 April 2024

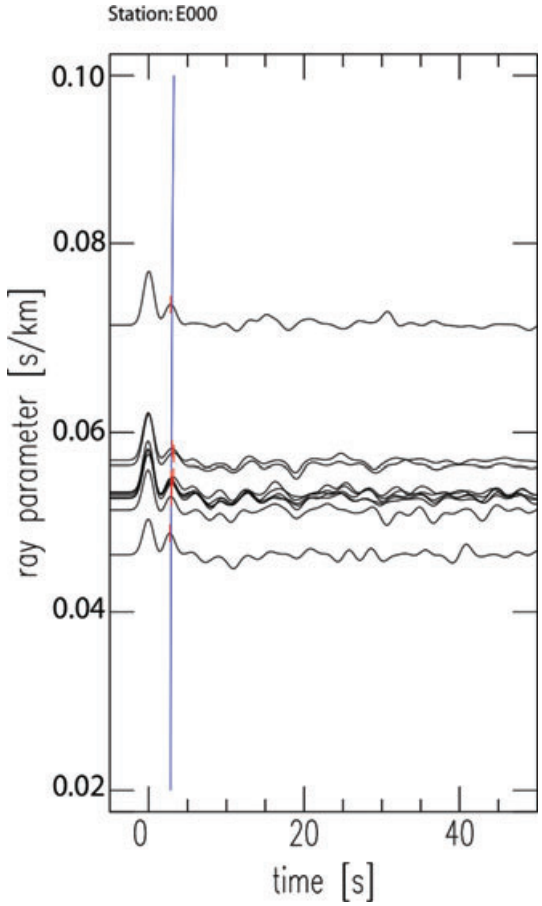

Figure 4. Receiver functions for station E000 arranged by ray parameter. The red marks show Moho P_s arrival times picked and the blue line shows the Moho P_s arrival time for the crustal thickness given in Table 2.

the higher average crustal V_s (∼3.9 km s^{-1}) in our model. Lawrence *et al*. (2006b) did not attempt to constrain the crustal V_p/V_s in their models.

Comparisons with the results obtained by Pondrelli *et al*. (1997) show that our crustal thickness estimates are consistent beneath the crest of the TAM, but our results are ∼8 km thicker along the coast. The difference in crustal thickness estimates may reflect the small number (4) of events used by Pondrelli *et al*. (1997) in their analysis. In contrast, our results are consistent with the seismic refraction profile published by Della Vedova *et al*. (1997), which shows ∼40 km thick crust under the crest of the TAM and ∼30 km thick crust under the coast.

Our crustal thickness estimate for station SBA on Ross Island of ∼27 km is 7 km thicker than the estimates from Bannister *et al*. (2003) and Lawrence *et al*. (2006b). Bannister *et al*. (2003) reported a Moho depth of ∼20 km by choosing the depth at which the *S*-wave velocity reached 4.2–4.3 km s^{-1} in their model, but they noted that the Moho structure in their model is gradational. Their model also shows an increase in *S*-wave velocity to 4.3–4.4 km s^{-1} at ∼28 km depth. Similarly, Lawrence *et al*. (2006b) reported a Moho depth of ∼20 km for SBA based on the depth in their velocity model at which the *S*-wave velocity increased to 4.15–4.35 km s^{-1}. Consistent with Bannister *et al*. (2003), in the Lawrence *et al*. (2006b) velocity model there is another *S*-wave velocity increase to 4.35–4.5 km s^{-1} at ∼26 km. If the deeper discontinuity (∼26–28 km depth) in the Bannister *et al*. (2003) and Lawrence *et al*. (2006b) models is selected as the Moho, then there is little discrepancy in the results between the three studies.

For station SBA, if we force the H–κ stacking algorithm to give a Moho depth of 20–22 km, which can be done by limiting the time window over which the algorithm is able to pick a Moho P_s, then we obtain a V_p/V_s value of 1.59, which is unrealistically low. Placing the Moho at 27 km depth instead of 20 km yields both a good fit to the RFs and a V_p/V_s value that is consistent with the composition of the volcanics on Ross Island, and therefore we argue that 27 km is a better estimate of crustal thickness than 20 km beneath station SBA.

For the other two stations on Ross Island, CBRI and CCRZ, we obtained Moho depth estimates of 19 and 25 km, respectively (Table 2). Within the reported uncertainty, our crustal thickness estimate for CBRI is consistent with the estimate from Lawrence *et al*. (2006b) and with the estimate from Bannister *et al*. (2003) for a nearby station. For station CCRZ, our Moho depth estimate is also consistent with the estimate from Lawrence *et al*. (2006b), given the reported uncertainties for our Moho depth estimate.

We obtained a crustal thickness estimate of ∼30 km for MINN, which is ∼10 km thicker than the estimate of Lawrence *et al*. (2006b). This discrepancy in Moho depth can be attributed to the selection of the Moho P_s arrival on the RFs. Lawrence *et al*. (2006b) identified the Moho P_s arrival at ∼3.3 s on their higher frequency RFs while we identified a Moho P_s at ∼4.2 s on our lower frequency RFs, which is consistent with the lower frequency RF from Lawrence *et al*. (2006b). If we force the H–κ algorithm to select the arrival at 3.3 s to be the Moho P_s using the higher frequency RFs, then the H–κ stacking algorithm yields two maxima in the objective function, one with a V_p/V_s value of 1.74 and a Moho depth of 30 km, and a second one with a V_p/V_s value of 1.64 and a Moho depth at 34 km. Given this result, we argue for a Moho depth of 30 km beneath station MINN.

5 SUMMARY AND CONCLUSIONS

In summary, V_p/V_s values for stations in the TAM situated away from the LVZ in the upper-mantle range from 1.63 to 1.78, with a mean of 1.73, while values for stations in the TAM lying above the LVZ and closer to the EVP range from 1.67 to 1.78, with a mean of 1.72. On Ross Island, a V_p/V_s value of 1.88 was obtained. Crustal thickness estimates along the Coastal array vary from 18 to 33 km, and along the East–West array they range from 25 km near the coast to 39 km beneath the crest of the TAM. On Ross Island, crustal thickness beneath stations CBRI is ∼19 km and increases to ∼27 and ∼25 km beneath stations SBA and CCRZ, respectively.

A comparison of the V_p/V_s values shows that there is little difference in bulk crustal composition for areas above and away from the LVZ, and together with a mean V_p/V_s value (1.72) typical for felsic to intermediate composition crust, suggests that the crust along the TAM front has not been altered significantly by mafic magmatism. If a significant portion of the crust had been modified by mafic intrusions and/or underplating, then V_p/V_s values closer to the V_p/V_s ratio of 1.88 found at Station SBA would be expected across areas of the TAM front lying above the LVZ. While a few kilometres of lower crustal modification cannot be ruled out, larger amounts of crustal modification by mafic intrusions and/or underplating are not consistent with the nature of the arrivals on the RFs or with the V_p/V_s values obtained.

Comparison to previous work indicates that along the Coastal array, our estimates of crustal thickness are 8–10 km thicker than

Downloaded from https://academic.oup.com/gji/article/185/1/85/606263 by guest on 09 April 2024

Table 1. Results from H–κ stacking method using crustal V_p of 6.5 km s^{-1}.

Station	H (km)	Uncertainty ± kilometre	Total uncertainty[a] ± kilometre	V_p/V_s	Uncertainty	Total uncertainty[a]	N
MAGL	33	0.4	4.7	1.67	0.03	0.04	19
CTEA	30	0.7	1.8	1.78	0.04	0.05	12
DIHI	33	1.0	2.2	1.63	0.04	0.05	19
E004	34	0.3	1.1	1.76	0.01	0.02	43
E006	30	2.1	3.2	1.70	0.09	0.10	7
E008	38	1.3	2.6	1.75	0.05	0.06	26
E010	39	0.6	2.0	1.77	0.02	0.03	16
N000	39	1.2	2.6	1.70	0.05	0.06	10
VNDA	35	0.1	1.4	1.78	0.01	0.02	276
SBA	27	0.3	1.3	1.88	0.01	0.02	347

Note: *N,* number of RFs.
[a]Combination of uncertainty from bootstrap and from varying crustal V_p in H–κ stacking.

Table 2. Summary of H estimates using the method of Zandt *et al*. (1995).

Station	H (km)	V_p/V_s	N
CPHI	32 ± 5.2	1.73	5
CBOB	30 ± 7.4	1.73	5
CASE	24 ± 3.5	1.73	5
MINN[a]	30 ± 2.4	1.88	10
CBRI[a]	19 ± 2.7	1.88	15
CCRZ[a]	25 ± 4.5	1.88	4
E000	25 ± 2.5	1.73	10
E002	27 ± 3.0	1.73	19
TNV	18 ± 5.0	1.73	18

Note: *N*, Number of RFs.
[a]Stations located in EVP.

the estimates from Lawrence *et al*. (2006b), except for stations TNV and CASE. Along the East–West array our results match well with Lawrence *et al*. (2006b) and Bannister *et al*. (2003), except at the coast, where our crustal thickness estimate is ∼5 km thicker. In addition, at stations SBA and CCRZ on Ross Island, we obtain a crustal thickness that is ∼5–7 km thicker than previously estimated. The difference in crustal thickness estimates possibly reflects the use by Lawrence *et al*. (2006b) and Bannister *et al*. (2003) of a lower V_s to define the Moho than we used, and by the low average crustal V_s used by Lawrence *et al*. (2006b) compared to the V_s we used.

Our results also indicate that the crust along the TAM front is quite variable, and, in many locations thicker than previously estimated. Bannister *et al*. (2003) and Lawrence *et al*. (2006b) suggested that there is an abrupt change in crustal thickness from ∼20 km at the coast to ∼40 km beneath the TAM near Ross Island. Our results show an increase in crustal thickness as well, but it is not quite as pronounced, increasing only from ∼25 km at the coast to ∼40 km beneath the TAM. This finding is consistent with the crustal model of Della Vedova *et al*. (1997) developed from seismic refraction data. However, elsewhere along the TAM front (i.e. station TNV), the crust is only 18 km thick.

ACKNOWLEDGMENTS

We thank W. Geissler and an anonymous reviewer for constructive comments. This research has been supported by the National Science Foundation (grants OPP 9909603 and OPP 9909648).

REFERENCES

Bannister, S., Yu, J., Leitner, B. & Kenett, B.L., 2003. Variations in crustal structure across the transition from West to East Antarctica, Southern Victoria Land, *Geophys. J. Int.,* **155,** 870–884.

Barrett, P.J., Elliot, D.H. & Lindsey, J.F., 1986. The Beacon Supergroup (Devonian- Triassic) and Ferrar Group (Jurassic) in the Beardmore Glacier area, Antarctica, in *Geology of the Central Transantarctic Mountains, Antarct. Res. Ser.,* Vol. 36, pp. 339–428, eds Turner, M.D. & Splettstoesser, J.F., AGU, Washington, D.C..

Behrendt, J.C., Duerbaum, H.J., Damaske, D., Saltus, R., Bosum, W. & Cooper, A.K., 1991a. Extensive volcanism and related tectonism beneath the Ross Sea continental shelf, Antarctica: interpretation of an aeromagnetic survey, in *Geo-logical Evolution of Antarctica,* pp. 299–304, ed. Thomson, J.W., Cambridge University Press, New York.

Behrendt, J.C., Le Masurier, W.E., Cooper, A.K., Tessensohn, F., Trehu, A., Damaske, D., 1991b. Geophysical studies of the West Antarctic Rift System, *Tectonics,* **10**(6), 1257–1273.

Behrendt, J.C., Saltus, R., Damaske, D., McCafferty, A., Finn, C.A., Blankenship, D. & Bell, R.E., 1996. Patters of late Cenozoic volcanic and tectonic activity in the West Antarctic Rift system revealed by aeromagnetic surveys, *Tectonics,* **15,** 660–676.

Christensen, N.I., 1996. Poisson's ratio and crustal seismology, *J. geophys. Res,* **101,** 3139–3156.

Cooper, A.F., Adam, L.J., Coulter, R.F., Eby, G.N. & McIntosh, W.C., 2007. Geology, geochronology and geochemistry of basanitic volcano, White Island, Ross Sea, Antarctica, *J. Volc. Geotherm. Res.,* **165,** 189–216.

Cooper, A.K., Davey, F.J. & Behrendt, J.C., 1987. Seismic stratigraphy and structure of the Victoria Land Basin, Western Ross Sea, Antarctica, in *The Antarctic Continental Margin: Geology and Geophysics of the Western Ross Sea,* Vol. 5B, pp 27–76, eds Cooper, A.K. & Davey, F.J., Earth Science Series, Houston, Texas, Circum-Pacific Council for Energy and Natural Resources.

Della Vedova, B., Pellis, G., Trey, H., Zhang, J., Cooper, A.K., Makris, J. & the ACRUP working group, 1997. Crustal structure of the Transantarctic Mountains, Western Ross Sea, in *The Antarctic Region: Geological Evolution and Processes,* pp.609–618, ed. Ricci, C.A., Terra Antarctica Publication, Siena.

Dugda, M.T., Nyblade, A.A., Julia, J., Langston, C.A., Ammon, C.J. & Simiyu, S., 2005. Crustal structure in Ethiopia and Kenya from receiver function analysis: implications for rift development in eastern Africa, *J. geophys. Res.*, **110,** B01303, doi:10.1029/2004JB003065

Efron, B. & Tibshirani, R., 1991, Statistical data analysis in the computer age, *Science,* **253,** 390–395.

Finotello, M., 2009. Crustal structure along the Transantarctic Mountain front using receiver functions, *M.S. thesis*. Pennsylvania State University, Pennsylvania, pp. 86.

Fitzgerald, P.G., 1992. The Transantarctic Mountains of Southern Victoria Land: the application of apatite fission track analysis to a rift shoulder uplift, *Tectonics,* **11**(3), 634–662.

Fitzgerald, P.G., 1994. Thermochronologic constraints on post-Paleozoic tectonic evolution of the central Transantarctic Mountains, Antarctica, *Tectonics,* **13,** 818–836.

Kyle, P.R., 1990a. McMurdo Volanic Group, western Ross Embayment: introduction, in *Volcanoes of the Antarctic Plate and Southern Ocean,*

Downloaded from https://academic.oup.com/gji/article/185/1/85/606263 by guest on 09 April 2024

Antarctic Research Series, Vol. 48, pp.19–15, eds LeMasurier, W.E. & Thomson, J.W., American Geophysical Union, Washington, DC.

Kyle, P.R., 1990b. Erebus Volcanic Province, in *Volcanoes of the Antarctic Plate and Southern Ocean, Antarctic Research Series*, Vol. 48, pp. 81–88, eds LeMasurier, W.E. & Thomson, J.W., American Geophysical Union, Washington, DC.

Kyle, P.R., Moore, J.A. & Thirlwall, M.F., 1992. Petrologic evolution of anorthoclase phonolite lavas at Mount Erebus, Ross Island, Antarctica, *J. Petrol.,* **33**(4), 849–875.

Langston, C.A., 1979. Structure under Mount Rainier, Washington, inferred from teleseismic body waves, *J. geophys. Res.,* **84,** 4749–4762.

Lawrence, J.F., Wiens, D.A., Nyblade, A.A., Anandakrishnan, S., Shore, P.J. & Voigt, D., 2006a. Rayleigh wave phase velocity analysis of the Ross Sea, Transantarctic Mountains, and East Antarctic from a temporary seismograph array, *J. geophys. Res.,* B06302, doi:10.1029/2005JB003812.

Lawrence, J.F., Wiens, D.A., Nyblade, A.A., Anandakrishnan, S., Shore, P.J. & Voigt, D., 2006b. Crust and upper mantle structure of the Transantarctic Mountains and surrounding regions from receiver functions, surface waves, and gravity: implications for uplift models, *Geochem. Geophys. Geosyst.,* **7,** Q10011, doi:10.1029/2006GC001282.

Ligorría, J.P. & Ammon, C.J., 1999. Iterative deconvolution and receiver function estimation, *Bull. seism. Soc. Am.,* **89,** 1395–1400.

Park, J. & Levin, V., 2000. Receiver functions from multiple-taper spectral correlation estimates, *Bull. seism. Soc. Am.,* **90,** 1507–1520.

Paulsen, T.S. & Wilson, T.J., 2009. Structure and age of volcanic fissures on Mount Morning: a new constraint on Neogene to contemporary stress in the West Antarctic Rift, southern Victoria Land, Antarctica, *Geol. Soc. Am. Bull.,* **121,** 1071–1088.

Pondrelli, S., Amato, A., Chiappini, M., Cimini, G.B., Colombo, D. & Bona, M. D., 1997. ACRUP1 Geotraverse: contribution of teleseismic data recorded on land, in *The Antarctic Region: Geological Evolution and Processes,* pp. 631–635, ed. Ricci, C.A., Terra Antarctica, Siena, Italy.

Trey, H., Cooper, A.K., Pellis, G., della Vedova, B., Cochrane, G., Brancolini, G. & Makris, J., 1999. Transect across the West Antarctic rift system in the Ross Sea, Antarctica, *Tectonophysics,* **301,** 61–74.

Watson, T., Nyblade, A., Wiens, D. A., Anandakrishnan, S., Benoit, M., Shore, P.J., Voigt, D. & VanDecar, J., 2006. P and S velocity structure of the upper mantle beneath the Transantarctic Mountains, East Antarctic craton, and Ross Sea from travel time tomography, *Geochem. Geophys. Geosyst.,* **7,** Q07005, doi:10.1029/2005GC001238.

Zandt, G., Myers, S.C. & Wallace, T.C., 1995. Crust and mantle structure across the Basin and Range-Colorado Plateau boundary at 37°N latitude and implications for Cenozoic extensional mechanism, *J. geophys. Res.,* **100**(10), 529–10548.

Zhu, L. & Kanamori, H., 2000. Moho depth variation in southern California from teleseismic receiver functions, *J. geophys. Res.,* **105,** 2969–2980.

SUPPORTING INFORMATION

Additional Supporting Information may be found in the online version of this article:

Station locations

Part A. H–κ stacking results for stations in Table 1. Mean crustal V_p and selection of weights used for stacking are explained in the text. Arrival times of Moho P_s and crustal multiples predicted by the H–κ results are indicated on the receiver functions.

Part B. Receiver functions plotted against ray parameter for stations in Table 2. Receiver functions shown were obtained using a Gaussian filter of 1.0 except for stations CCRZ and CBRI, where a Gaussian of 2.5 was used.

Part C. Azimuthal data coverage illustrated on figures showing Moho P_s conversion points (red symbols) for receiver functions used in this study. Small maps show conversion point locations for individual stations.

Please note: Wiley-Blackwell are not responsible for the content or functionality of any supporting materials supplied by the authors. Any queries (other than missing material) should be directed to the corresponding author for the article.

Downloaded from https://academic.oup.com/gji/article/185/1/85/606263 by guest on 09 April 2024